Images as Manifolds Embedded in a Spatial–Feature Non-Euclidean Space

Nir Sochen and Yehoshua Y. Zeevi
Department of Electrical Engineering
Technion-Israel Institute of Technology
Haifa 32000, Israel.

November 29, 1998

Abstract

In image analysis, processing and understanding, it is highly desirable to be able to process images and feature domains by methods that are specific to these domains. We show how the geometrical framework of scale-space flows is most convenient for this purpose, and demonstrate, as an example, how different models of color perception can be interpreted as different geometries of the color space and result in a variety of processing schemes. We go beyond these models and show how one can switch locally between the L_1 and L_2 norms for different processing flows of spatial and color domains. The parameter that interpolates between the norms is the magnitude of contrast/luminance, taken here as a local function of the image embedding space. The resulting spatial and grey level/luminance preserving flow, can be used for conditional denoising and segmentation. These examples demonstrate that the proposed framework can incorporate context or task-related data, furnished by either the human user or an active vision subsystem in a coherent and convenient way.

1 Introduction

In a variety of applications of denoising, smoothing and enhancement of images, it is advantageous to have simple and automatic "buttons" that enable control the local smoothing of an image or feature space according to some a priori knowledge of the class of images to be processed and the task at hand.

We present and implement a method that employs the recently-proposed geometric Beltrami framework for non-linear scale-space methods [12]. According to this framework, an image is treated as an embedding of a manifold in a higher dimensional spatial-feature manifold. The embedding manifold is a hybrid space that combines spatial coordinates and a variety of feature coordinates. The features may include apart from intensity and color, elements of the intensity jet bundle (basically derivatives of the intensity), wavelets' parameters like typical local size and orientation, statistical nd others characteristics. The choice of the appropriate embedding space depends on the

class of images to be processed and the nature of the task. The knowledge about the task and the nature of the feature space is encoded in the geometry of the embedding space.

This study is devoted to grey level and color images. Textures will be dealt with separately [13]. A grey level image is considered according to the proposed framework as a two-dimensional surface (i.e. the graph of $I(x,y)$), **embedded** in the three-dimensional space whose coordinates are (x,y,I). Likewise, a color image is considered as a two-dimensional surface **embedded** in the five-dimensional space whose coordinates are (x,y,U_1,U_2,U_3), where (U_1,U_2,U_3) are color coordinates (e.g. $(U_1,U_2,U_3)=(R,G,B)$). Color space and its perception is an issue that has fascinated researchers for over a century. It is natural, from our viewpoint, to apply our framework to this class of color images since the knowledge accumulated along the years is integrated into and encoded in the geometry of the color space. This form is especially convenient and readily available to use in the Beltrami framework.

It was suggested [12], that the nonlinear scale space can be treated as a gradient descent with respect to a functional that depends on the geometry (i.e. the metric) of the image surface, as well as on the embedding and the geometry of the embedding space. In the examples treated previously, it was assumed that the embedding space is Euclidean and that the system of coordinates that describes it is Cartesian [12], [4]. In fact, the geometry of the embedding space is flexible and can be determined according to an a priory knowledge about the class of images to be processed and the high level task that one has in mind. We view the geometry of the embedding space as the interface between the high-level task, the a priory knowledge and the low-level process to be implemented.

The simplest and most intuitive example, where a high level constraint is introduced via a change in the embedding space geometry, is the adaptive smoothing of a grey-level image according to different illumination conditions. This is achieved by having an intensity-dependent embedding space geometry. We treat grey level images as an embedding of a 2D surface in a 3D space whose coordinates are (x,y,I). We then control locally in x,y, and I the contrast normalization ratio that parameterizes the way we choose to normalize the feature coordinate I with respect to the spatial coordinates x and y. Making the contrast normalization ratio a local function of (x,y,I) enables us to control the rate of diffusion in the spatial (i.e. x and y) domain as well as along the feature coordinate I. A similar idea, of controlling locally the gain in the image acquisition formation process, was used by Zeevi et al. [19][20].

Another well-known example is the geometry of the color space. Research related to this issue started more than a hundred years ago and various geometrical and statistical methods were applied in order to resolve it. We show here how the knowledge accumulated is naturally incorporated in the geometrical framework.

The grey level technique and color space information can be combined and naturally generalized to treat colored images in cases where a different noise is encountered in each of the color channels. A different PDE algorithm was utilized in [3], but with no coupling between the different color channels.

The paper is organized as follows: Section 2 reviews approaches to the geometry of the color space. Section 3 presents the geometrical framework for scale space, following the approach presented in [12]. The Beltrami flow, which results from the geometric framework, and integrates the information presented in Section 2 into a practical tool

of denoising, is presented in Section 4. In Section 5 we study the possibility to gauge locally the importance of the feature space with respect to the spatial space. Both, grey-level and color analysis are carried out in details. Section 6 deals with the numerical implementation of the method and presents results. In Section 7 we discuss the potential for further research. In order to be self-contained we review in the appendix the Riemannian geometric definitions, terminology and theorems used in this study.

2 Color Space Geometry

Two questions should be addressed in the process of evaluating the geometry of the color space. The first relates to the variables (or coordinates), and the second to the geometry of the color space. Attempts to describe color perception geometry go back more than a hundred years. Helmholtz [2] was the first to define a 'line element' (arclength) in color space. He first used a Euclidean R, G, B space defined by the arclength

$$ds^2 = (c_R d\log R)^2 + (c_G d\log G)^2 + (c_B d\log B)^2. \tag{1}$$

His first model failed to represent faithfully empirical data of human color perception. Schrödinger [10] improved the model of Helmholtz by introducing the arclength

$$ds^2 = \frac{1}{c_R R + c_G G + c_B B}\left(\frac{c_R(dR)^2}{R} + \frac{c_G(dG)^2}{G} + \frac{c_B(dB)^2}{B}\right), \tag{2}$$

where c_R, c_G, c_B are constants. Schrödinger's model was later found to be inconsistent with findings on threshold data of color discrimination.

Koenderink et al. [5] generalized these line elements and incorporated a family of metrics

$$ds^2 = (c_R R + c_G G + c_B B)^{\alpha-2}\left(\frac{c_R(dR)^2}{R^\alpha} + \frac{c_G(dG)^2}{G^\alpha} + \frac{c_B(dB)^2}{B^\alpha}\right), \tag{3}$$

where different values of α correspond to different models: $\alpha = 2$ is the Helmholtz model, $\alpha = 1$ is Schrödinger's. Koenderink et al. studied the case of $\alpha = 0$.

Stiles at al. advocated another generalization of the Helmholtz line element

$$ds^2 = (c_R d\log(aR + b))^2 + (c_G d\log(aG + b))^2 + (c_B d\log(aB + b))^2, \tag{4}$$

with a, b being constants. Other analytical attempts culminated in the Vos-Walraven line element [16]

$$\begin{aligned}
ds^2 &= (dR)^2\left[\eta_L f_L + \eta_F f_F G^2(1+\frac{G}{G_0})^2 + \eta_s f_s B^2(1+\frac{G}{G_0})^2\right] \\
&+ (dG)^2\left[\eta_L f_L + \eta_F f_F R^2(1+\frac{R}{R_0})^2 + \eta_s f_s B^2(1+\frac{B}{B_0})^2\right] \\
&+ (dB)^2\left[\eta_L f_L + \eta_s f_s Y^2(1+\frac{Y}{Y_0})^2\right] \\
&+ 2dRdG\left[\eta_L f_L - \eta_F f_F R(1+\frac{R}{R_0})G(1+\frac{G}{G_0}) + \eta_s f_s B^2(1+\frac{B}{B_0})^2\right] \\
&+ 2dRdB\left[\eta_L f_L - \eta_s f_s B(1+\frac{B}{B_0})Y(1+\frac{Y}{Y_0})\right]
\end{aligned}$$

$$+ \quad 2dGdB\left[\eta_L f_L - \eta_s f_s B(1+\frac{B}{B_0})Y(1+\frac{Y}{Y_0})\right], \tag{5}$$

with $Y = R + G$, η_L, η_F, η_s are constants, and

$$\begin{aligned}
f_s &= \frac{\frac{B}{1+B/B_0+B^3/B_1^3} + \frac{Y}{1+Y/Y_0+Y^3/Y_1^3}}{\left[\frac{B(1-B/B_0)}{1+B/B_0+B^3/B_1^3} + \frac{Y(1+Y/Y_0)}{1+Y/Y_0+Y^3/Y_1^3}\right]^2 (1+\frac{Y}{Y_0}+\frac{Y^3}{Y_1^3})(1+\frac{B}{B_0}+\frac{B^3}{B_1^3})YB} \\
f_F &= \frac{\frac{B}{1+G/G_0+G^3/G_1^3} + \frac{R}{1+R/R_0+R^3/R_1^3}}{\left[\frac{G(1-G/G_0)}{1+G/G_0+G^3/G_1^3} + \frac{R(1+R/R_0)}{1+R/R_0+R^3/R_1^3}\right]^2 (1+\frac{R}{R_0}+\frac{R^3}{R_1^3})(1+\frac{G}{G_0}+\frac{G^3}{G_1^3})RG} \\
f_L &= \frac{1}{L(1+L/L_0+L^3/L_1^3)}
\end{aligned} \tag{6}$$

with $L = R + G + B$.

MacAdams constructed an empirical line element based on direct psychophysical experimental results. His result can be given in tables and graphs only. The theoretical challenge is the construction of an analytical line element that is compatible with the features of the entire color perception space found in MacAdams' experimental data.

Summarizing the classes of existing models for color space, we have two main cases:

- The *inductive* line elements that derive the arclength by simple assumptions on the visual response mechanisms. For example, we can assume that the color space can be simplified and represented as a Riemannian space with zero Gaussian curvature, e.g. Helmholtz [2] or Stiles [15][18] models. Another possibility for inductive line elements is to consider color arclengths like Schrödinger or Vos-Walraven [16]. These models define color spaces with non zero curvature ('effective' arclength).
- The *empirical* line elements, in which the metric coefficients are determined to fit empirical data. Some of these models describe a Euclidean space like the CIELAB (CIE 1976 ($L^*a^*b^*$)) [18], recently used in [9]. Others, like MacAdam [6][7], are based on an effective arclength.

An alternative possible approach is to use statistical methods. Since the basic colors red, green and blue are correlated in most natural images, we can adopt the Buchsbaum [1] and the Wolf-Ginosar-Zeevi approach [17], and apply the KLT to obtain an uncorrelated basis k_1, k_2 and k_3. Denoting by I^a the three color planes, where a =r, g, b, the autocorrelation matrix is

$$\Phi^{ab} = \frac{1}{NM}\sum_{i=1}^{N}\sum_{j=1}^{M}\tilde{I}_{ij}^a\tilde{I}_{ij}^b, \tag{7}$$

where $\tilde{I}^a$ is the the channel value shifted by the mean. The autocorrelation matrix was found for a family of outdoors scenes and diagonalized. The transformation from R, G, B to the new basis is given explicitly by [17]:

$$\begin{pmatrix} k_1 \\ k_2 \\ k_3 \end{pmatrix} = \begin{pmatrix} 0.3744 & 0.4452 & 0.8103 \\ -0.3249 & -0.1195 & 0.0753 \\ 0.0051 & 0.0012 & 0.0002 \end{pmatrix} \begin{pmatrix} R \\ G \\ B \end{pmatrix}. \tag{8}$$

where k_s are the eigenvectors of the autocorrelation matrix. The coordinates used by us are (after defining $x = \sigma^1$ and $y = \sigma^2$)

$$(x, y, k_1(x,y), k_2(x,y), k_3(x,y)). \tag{9}$$

The k_1 coordinate represents the achromatic channel of luminance, while k_2 and k_3 are red-green and blue-yellow chromatic channels.

3 The Differential Geometric framework

This framework of image presentation and analysis is based on geometrical ideas adopted from general relativity and high energy physics. The essence of the method can be summarized as follows:

- An image is considered to be a Riemannian manifold embedded in a higher dimensional Riemannian manifold which is called the spatial-feature manifold. A two-dimensional image is according to this viewpoint a Riemannian surface. Let introduce on the nonlinear surface a local coordinate system (σ^1, σ^2). The embedding of this surface in, for example, a three-dimensional space with coordinates (X^1, X^2, X^3), is realized by specifying, for each point of the surface, the three-dimensional coordinates, namely:

$$(X^1(\sigma^1, \sigma^2), X^2(\sigma^1, \sigma^2), X^3(\sigma^1, \sigma^2)).$$

  Let M denote the higher dimensional spatial-feature manifold. We introduce, in general, a one-parameter family of embedded images $(X^i(\sigma^1, \sigma^2; t))_{i=1}^{\dim M}$, where t is the independent variable of the evolution, called the scale or "time". This parameter determines the degree of blurring or denoising of the image.

- From a geometrical viewpoint this family of embedded images describes a flow of a two-dimensional surface within a higher dimensional space. The dynamics of the surface flow is governed by a nonlinear heat-type partial differential equation applied to this one-parameter family of images. The equation is derived as a gradient descent of a functional that weight embedding maps in a geometrical way. It gives a precise control on the direction and amount of diffusion at each point of the image surface. This is to be compared with linear scale-space that diffuses "blindly" or the Perona-Malik equation that has a local control on the amount of diffusion but not on its direction.

We turn now to a rigorous treatment of these ideas and present the technical tools implemented in the sequel. A precise definition of a manifold and its geometry are incorporated. Next a measure on the space of embedding maps is introduced. The measure, or the energy functional, depends on the geometry of the spaces involved and is independent of the coordinate system selected to describe these manifolds.

3.1 The Induced Metric

Let $\mathbf{X} : \Sigma \to M$ be an embedding of $(\Sigma, (g_{\mu\nu}))$ in $(M, (h_{ij}))$, where Σ and M are Riemannian manifolds and $(g_{\mu\nu})$ and (h_{ij}) are their metrics respectively. We can use the knowledge of the metric on M and the map $\mathbf{X}$ to construct the metric on Σ. This procedure, denoted formally by $(g_{\mu\nu})_\Sigma = \mathbf{X}^*(h_{ij})_M$ and called the *pullback*, is given explicitly as follows:

$$g_{\mu\nu}(\sigma^1, \sigma^2) = h_{ij}(\mathbf{X}) \partial_\mu X^i \partial_\nu X^j, \tag{10}$$

where $i,j = 1,...,\dim M$ are being summed over, using the Einstein summation convention, and $\partial_\mu X^i \equiv \partial X^i(\sigma^1,\sigma^2)/\partial\sigma^\mu$.

3.2 The Measure On Maps

The diffusion equation to be used is derived as a gradient descent of an action functional. The functional in question depends on *both* the image manifold and the embedding space. Denote by $(\Sigma,(g_{\mu\nu}))$ the image manifold and its metric, and by $(M,(h_{ij}))$ the spatial-feature manifold and its metric. Then, the mapping $\mathbf{X}:\Sigma\to M$ is presented by the action [8]:

$$S[X^i,g_{\mu\nu},h_{ij}] = \int d^m\sigma\sqrt{g}g^{\mu\nu}\partial_\mu X^i\partial_\nu X^j h_{ij}(\mathbf{X}), \tag{11}$$

where m is the dimension of Σ, g is the determinant of the image metric and $g^{\mu\nu}$ is the inverse of the image metric. The range of indices is $\mu,\nu = 1,\dots,\dim\Sigma$, and $i,j = 1,\dots,\dim M$. The metric of the embedding space is h_{ij}.

The Polyakov action is a generalization of the L_2 norm to curved spaces. Here, $d^m\sigma\sqrt{g}$ is the volume element (area element for d=2) of Σ - the image manifold, and $g^{\mu\nu}\partial_\mu X^i\partial_\nu X^j h_{ij}(\mathbf{X})$ is the generalization of $|\nabla I|^2$ to maps between non-Euclidean manifolds. Note that the volume element as well as the rest of the expression is invariant under reparameterization, that is, $\sigma^\mu\to\tilde{\sigma}^\mu(\sigma^1,\sigma^2)$. The Polyakov action depends, actually, on the geometry and not on the way we describe the objects via our parameterization of the coordinates. In other words the resultant value of the functional does not depend on the choice of local coordinates.

3.3 The Gradient Descent Flow

Given the above functional, we have to choose the minimization criterion. We may choose, for example, to minimize the functional only with respect to the embedding. In this case the metric $g_{\mu\nu}$ is treated as a set of parameters that can be selected with reference to the application. Another choice is to minimize only with respect to the feature coordinates of the embedding space, or one may choose to minimize the image metric as well. Each of these choices yields a different flow. Some flows are, in fact, identical to existing methods like the heat flow, the Perona-Malik flow, or the mean-curvature flow. Other choices are new and will be described below in detail.

Another important point is the choice of the embedding space and its geometry. In general, we need information about the task at hand in order to fix the right geometry.

Using standard methods in variational calculus, the Euler-Lagrange (EL) equations, with respect to the embedding, are (see [12] for derivation):

$$-\frac{1}{2\sqrt{g}}h^{il}\frac{\delta S}{\delta X^l} = \frac{1}{\sqrt{g}}\partial_\mu(\sqrt{g}g^{\mu\nu}\partial_\nu X^i) + \Gamma^i_{jk}\partial_\mu X^j\partial_\nu X^k g^{\mu\nu}, \tag{12}$$

where Γ^i_{jk} are the Levi-Civita connection coefficients, with respect to the spatial-feature metric h_{ij}, defined as (see Appendix A):

$$\Gamma^i_{jk} = \frac{1}{2}h^{il}(\partial_j h_{lk} + \partial_k h_{jl} - \partial_l h_{jk}). \tag{13}$$

The second term in Eq. (12) is due to the non-linear geometry of the embedding space.

We view the scale-space as a gradient descent:

$$X^i_t \equiv \frac{\partial X^i}{\partial t} = -\frac{1}{2\sqrt{g}} h^{il} \frac{\delta S}{\delta X^l}. \tag{14}$$

A few remarks are in order. First, note that we took the freedom to multiply the EL equations by a strictly positive function and a positive definite matrix.

This factor is the simplest one that does not change the minimization solution, while giving a reparameterization invariant expression. This choice guarantees geometric flow and does not depend on the parameterization. The operator acting on X^i in the first term of Eq. (12) is the natural generalization of the Laplacian from flat spaces to manifolds, called the Laplace-Beltrami operator, or in short *Beltrami operator*, denoted by Δ_g. When the embedding is in a Euclidean space with a Cartesian coordinate system, the connection elements are zero. If the embedding space is not Euclidean, we have to include the Levi-Civita connection term since it is not identically zero any more.

4 The Beltrami Flow

The metric of the embedding space is composed from the spatial metric and the feature space metric as a direct sum. Namely:

$$ds^2 = ds^2_{spatial} + \beta ds^2_{feature}. \tag{15}$$

More general line elements for the spatial-feature space are, in principle, possible. One such possibility is to consider a non-constant β, such that the strength of the conjugation between the spatial and feature coordinates is locally fixed in spatial and/or image features. This generalization, treated below in Section 4, is one of the novelties of this study.

Other generalizations may include non-trivial metric elements that combine spatial and feature coordinates (i.e. non trivial coefficients of $dxdI$ for grey level images or $dydR$ for color images). Such further generalizations as well as numerical results will be reported elsewhere [13].

4.1 Grey Level Beltrami Flow

Consider grey level images, it is clear that the intensity I has to be considered differently from x and y. In fact, the relative scale of I with respect to the spatial coordinates (x, y) has to be specified. This can be interpreted as taking the following metric of the embedding space

$$(h_{ij}) = \begin{pmatrix} 1 & 0 & 0 \\ 0 & 1 & 0 \\ 0 & 0 & \beta^2 \end{pmatrix}. \tag{16}$$

We will see below that different limits of this ratio β interpolate between the flows that originate from the Euclidean L^1 and L^2 norms.

A grey level image is regarded as a map $f : \Sigma \to \mathbb{R}^3$, where Σ is a two-dimensional manifold, and the flow is natural in the sense that it minimizes the action functional

with respect to I and taking the metric (g_{ij}) as the induced metric Eq. (10). It is easy to verify that this flow is invariant under reparameterization. The coordinates X and Y are, according to this viewpoint, parameters determined as above by σ^1 and σ^2. The result of the minimization is the Beltrami operator acting on I:

$$I_t = \Delta_g I \equiv \frac{1}{\sqrt{g}}\partial_\mu(\sqrt{g}g^{\mu\nu}\partial_\nu I) = HN_{\hat{I}}, \tag{17}$$

where H is the mean curvature and $N_{\hat{I}}$ is the component, in the I direction, of the vector normal to the surface, given explicitly by the following expressions:

$$\begin{aligned} H &= \frac{(1+I_x^2)I_{yy} - 2I_xI_yI_{xy} + (1+I_y^2)I_{xx}}{g^{\frac{3}{2}}} \\ N &= \frac{1}{\sqrt{g}}(-I_y, -I_x, 1)^T, \end{aligned} \tag{18}$$

where $g = 1 + I_x^2 + I_y^2$.

The geometrical meaning is obvious; each point on the image surface moves with a velocity that depends on the mean curvature and the I component of the normal to the surface at that point. Since the normal to the surface along edges lies almost entirely in the X-Y plane, I changes very little along the edges while the flow drives other regions of the image towards a minimal surface in a more rapid rate.

4.2 Color Analysis

Similarly, to the above treatment of grey level images, in the case of for color images we minimize with respect to the color space coordinates, i.e. R,G,B or the KLT coordinates K_1, K_2, K_3. For the geometry we choose the following metric

$$ds^2 = dx^2 + dy^2 + \beta ds^2_{color}, \tag{19}$$

where β^2 is constant. Alternatively, for such a fixed β, we can say that the metric of the embedding space is

$$(h_{ij}) = \begin{pmatrix} 1 & 0 & 0 & 0 & 0 \\ 0 & 1 & 0 & 0 & 0 \\ 0 & 0 & \beta h_{rr} & \beta h_{rg} & \beta h_{rb} \\ 0 & 0 & \beta h_{gr} & \beta h_{gg} & \beta h_{gb} \\ 0 & 0 & \beta h_{br} & \beta h_{bg} & \beta h_{bb} \end{pmatrix}. \tag{20}$$

In the color spaces that we described in Section 2, all the metrics, but the Vos-Walraven one, were diagonal. Namely, they have the form:

$$(h_{ij}) = \begin{pmatrix} 1 & 0 & 0 & 0 & 0 \\ 0 & 1 & 0 & 0 & 0 \\ 0 & 0 & \beta h_{rr} & 0 & 0 \\ 0 & 0 & 0 & \beta h_{gg} & 0 \\ 0 & 0 & 0 & 0 & \beta h_{bb} \end{pmatrix}. \tag{21}$$

The induced metric elements are according to Eq. (10):

$$g_{11} = 1 + \beta(h_{rr}R_x^2 + h_{gg}G_x^2 + h_{bb}B_x^2)$$

$$
\begin{aligned}
g_{12} &= g_{21} = \beta(h_{rr}R_xR_y + h_{gg}G_xG_y + h_{bb}B_xB_y) \\
g_{22} &= 1 + \beta(h_{rr}R_y^2 + h_{gg}G_y^2 + h_{bb}B_y^2).
\end{aligned} \tag{22}
$$

Note also that this two-dimensional image-induced-metric is different from the one we had in the Euclidean case. It means that the choice of the color space geometry has a direct impact on the first term of the diffusion equation (i.e. $\frac{1}{\sqrt{g}}\partial_\mu(\sqrt{g}g^{\mu\nu}\partial_\nu X^i)$. This is not the only place where changes should be made. The second term which includes in this case non-trivial Levi-Civita connection coefficients, should be evaluated as well. We introduce the notation $\beta_i \equiv \beta h_{ii}$ for i = r,g,b and calculate the Levi-Civita coefficients. In our case h_{ij} is

$$
h_{ij} = \alpha_i \delta_{ij}\,. \tag{23}
$$

Using this explicit form in the general formula of Eq. (13), we get

$$
\Gamma^i_{jk} = \frac{1}{2}\alpha_i^{-1}(\partial_j\alpha_i\delta_{ik} + \partial_k\alpha_i\delta_{ij} - \partial_i\alpha_j\delta_{jk}), \tag{24}
$$

This means that a Levi-Civita coefficient is zero, unless one of the lower indices equals the upper one or the lower indices are equal. In the case of the Schrödinger model, we find:

$$
\alpha_i = \frac{1}{AI_i}, \tag{25}
$$

where $A = c_rR + c_gG + c_bB$. A short analysis yields for this model

$$
\Gamma^i_{jk} = \frac{c_jI_i}{2AI_j}\delta_{jk} - \frac{c_j}{2A}\delta_{ik} - \frac{c_k}{2A}\delta_{ij} - \frac{1}{2I_i}\delta_{ij}\delta_{ik}, \tag{26}
$$

or term by term:

$$
\begin{aligned}
\Gamma^r_{rr} &= -\frac{c_r}{2A} - \frac{1}{2I_r} \\
\Gamma^r_{rg} &= \Gamma^r_{gr} = -\frac{c_g}{2A} \\
\Gamma^r_{rb} &= \Gamma^r_{br} = -\frac{c_b}{2A} \\
\Gamma^r_{gg} &= \frac{c_gI_r}{2AI_g} \\
\Gamma^r_{bb} &= \frac{c_bI_r}{2AI_b},
\end{aligned} \tag{27}
$$

where all other non-zero elements are obtained by cyclic permutations of $\{r, g, b\}$.

Combining Eqs. (12), (14) and (26) we finally get the flow:

$$
\begin{aligned}
I^r_t = \Delta_g I^r \quad - \quad & (\frac{1}{2R} + \frac{c_r}{2A})(R_x^2g^{11} + 2R_xR_yg^{12} + R_y^2g^{22}) - \\
& \frac{c_g}{A}(R_xG_xg^{11} + (R_xG_y + R_yG_x)g^{12} + R_yG_yg^{22}) - \\
& \frac{c_b}{A}(R_xB_xg^{11} + (R_xB_y + R_yB_x)g^{12} + R_yB_yg^{22}) + \\
& \frac{c_gR}{2AG}(G_x^2g^{11} + 2G_xG_yg^{12} + G_y^2g^{22}) + \\
& \frac{c_bR}{2AB}(B_x^2g^{11} + 2B_xG_yg^{12} + B_y^2g^{22}),
\end{aligned} \tag{28}
$$

where

$$\begin{aligned}\Delta_g I^r &= \left(\frac{g_x g^{11}}{2g} + \frac{g_y g^{12}}{2g} + g_x^{11} + g_y^{12}\right) I_x^r + \\ &\left(\frac{g_x g^{12}}{2g} + \frac{g_y g^{22}}{2g} + g_x^{12} + g_y^{22}\right) I_y^r + \\ &g^{11} I^{xx} + 2g^{12} I_{xy}^r + g^{22} I_{yy}^r,\end{aligned} \tag{29}$$

$g_x^{ij} = \partial g^{ij}/\partial x$ ($g_y^{ij} = \partial g^{ij}/\partial y$) and $g_x = \partial g/\partial x$ ($g_y = \partial g/\partial y$).

A flow based on Stiles' line element is computed similarly. The line element suggested by Koenderink et al. is closely related to the local contrast normalization method and is treated in the next section.

5 Local Contrast Normalization

5.1 Analysis of Image Intensity

According to the above analysis there is an implicit parameter of the embedding procedure. So far we described the embedding as

$$\{X^1(\sigma^1,\sigma^2) = \sigma^1,\ X^2(\sigma^1,\sigma^2) = \sigma^2,\ X^3(\sigma^1,\sigma^2) = I(\sigma^1,\sigma^2)\}, \tag{30}$$

but actually the contrast normalization is arbitrary and could as well be chosen as

$$\tilde{X}^3(\sigma^1,\sigma^2) = \beta I(\sigma^1,\sigma^2). \tag{31}$$

In the latter case, the line element is

$$d\tilde{s}^2 = dx^2 + dy^2 + d(\tilde{X}^3)^2 = dx^2 + dy^2 + \beta^2 dI^2. \tag{32}$$

We interpret the scaling of the intensity as a change in the metric of the embedding space:

$$(h_{ij}) = \begin{pmatrix} 1 & 0 & 0 \\ 0 & 1 & 0 \\ 0 & 0 & \beta^2 \end{pmatrix}. \tag{33}$$

The limits of very large and very small β correspond to the L_1 and L_2 norms, respectively, as can be easily seen from the EL equations (12):

$$\begin{aligned}\lim_{\beta\to 0} EL(\beta) &= (I_{xx} + I_{yy}) = \frac{\delta L_2}{\delta I} \\ \lim_{\beta\to\infty} \beta^2 EL(\beta) &= \left(\frac{I_y^2 I_{xx} - 2I_x I_y I_{xy} + I_x^2 I_{yy}}{(I_x^2 + I_y^2)^2}\right) = \frac{\delta L_1}{\delta I}.\end{aligned} \tag{34}$$

The flows that result from these two limits in the form of $I_t = \mathrm{EL}(\beta)$ are very different in nature as can be seen in Fig. (1), where the two halves of the image were processed with different β ratios. In a large class of images, where intensity is not uniform and significant portions of the image are very bright or very dark, various regions should be treated differently. One should affect very little the dark regions by changing the inter pixel relationships, since processing destroys all the available information in those

Figure 1: Left: Original Lenna image. Right: Lenna processed with $\beta = 4.4$–left half and $\beta = 0.6$ right half.

regions, while brighter areas can be processed more "rapidly" (aggressively) without considerable loss of information. This can be achieved according to our formalism by considering the contrast to be a local function of (x, y, I) and interpreting it as an embedding of the image surface in a non-Euclidean three-dimensional manifold. Similar ideas, implementing different nonlinear formalism, underline the adaptive gain control processing reported by Zeevi et al. [19], [20].

The main idea is to let β be a **local** function of x, y and I such that various regions will be treated differently. As an example we choose a contrast normalization function $\beta(x, y, I)$ such that for dark regions β is large and the flow is L_1-like, while for more luminous regions β is small and the flow is L_2-like. There are many reasonable choices for the function β. We will use

$$\beta(x, y, I) = Ae^{-b_1(x-x_0)^2 - b_2(y-y_0)^2 - b_3(I-I_0)^2}, \tag{35}$$

with A and b's constants yet to be defined.

The effect of the function β is to impose slow diffusion within an ellipsoid with axes b_1, b_2 and b_3 around (x_0, y_0, I_0). More distant areas diffuse at the normal Beltrami rate while in very distant areas, where $\beta < 1$, the diffusion is faster then the Beltrami rate and approaches the linear scale-space rate. From a geometrical viewpoint, it amounts to choosing an appropriate embedding space. The metric of the embedding space is, under these circumstances, not constant:

$$h_{ij}) = \begin{pmatrix} 1 & 0 & 0 \\ 0 & 1 & 0 \\ 0 & 0 & \beta(x, y, I)^2 \end{pmatrix}. \tag{36}$$

This equation implies that the distance along the intensity axis depends on the point (x, y, I) where it is measured. In other words, our embedding space is not Euclidean any more.

As a consequence of the fact that we are working now on a curved manifold as our embedding manifold, we have to take into account that the Levi-Civita connection of our three-dimensional manifold does not vanish, and its contribution has to be added

according to the EL equation. Note also that the two-dimensional image induced metric is different from the one we had in the Euclidean case, since the induced metric depends on h_{ij} by Eq. (10). The first term of the EL reads:

$$\begin{aligned}\Delta_{g(\beta)} I &= \frac{1}{g^2}((1+\beta^2 I_x^2) I_{yy} - 2\beta^2 I_x I_y I_{xy} + (1+\beta^2 I_y^2) I_{xx} \\ &- \beta(\beta_x I_x + \beta_y I_y)(I_x^2 + I_y^2)), \end{aligned} \tag{37}$$

where $g = \det(g_{\mu\nu}) = 1 + \beta^2(I_x^2 + I_y^2)$.

The Levi-Civita connection coefficients are according to the definition (Appendix A)

$$\Gamma^i_{jk} = \frac{1}{2} h^{il}(\partial_j h_{lk} + \partial_k h_{jl} - \partial_l h_{jk}), \tag{38}$$

where there is an implicit sum over l. In our case h_{ij} is given by Eq. (36). Using the above definition, we get

$$\begin{aligned}\Gamma^1_{33} &= -\beta\beta_x \\ \Gamma^2_{33} &= -\beta\beta_y \\ \Gamma^3_{13} &= \beta^{-1}\beta_x \\ \Gamma^3_{23} &= \beta^{-1}\beta_y \\ \Gamma^3_{33} &= \beta^{-1}\beta_I, \end{aligned} \tag{39}$$

where all the other coefficients vanish. We can now calculate the second term of the El equations:

$$\begin{aligned}\Gamma^3_{ij}\partial_\mu X^i \partial_\nu X^j g^{\mu\nu} &= \Gamma^3_{11} g^{11} + 2\Gamma^3_{12} g^{12} + \Gamma^3_{22} g^{22} \\ &+ 2\Gamma^3_{13}(g^{11} I_x + g^{12} I_y) + 2\Gamma^3_{23}(g^{12} I_x + g^{22} I_y) \\ &+ \Gamma^3_{33}(g^{11} I_x^2 + 2 g^{12} I_x I_y + g^{22} I_y^2) \\ &= \frac{1}{\beta g}(2\beta_x I_x + 2\beta_y I_y + \beta_I(I_x^2 + I_y^2)). \end{aligned} \tag{40}$$

Collecting all the terms, we get the flow

$$\begin{aligned} I_t &= \frac{1}{g^2}((1+\beta^2 I_x^2) I_{yy} - 2\beta^2 I_x I_y I_{xy} + \\ &(1+\beta^2 I_y^2) I_{xx}) - \beta(\beta_x I_x + \beta_y I_y)(I_x^2 + I_y^2)) + \\ &\frac{1}{\beta g}\left(2\beta_x I_x + 2\beta_y I_y + \beta_I(I_x^2 + I_y^2)\right). \end{aligned} \tag{41}$$

This can be written in an explicit way by performing the derivatives on the function β given by Eq. (35).

5.2 Color

A local normalization constant for color images means a special choice of the line element:

$$ds^2 = dx^2 + dy^2 + \beta(U_1, U_2, U_3) ds^2_{color}, \tag{42}$$

where the U's are the coordinates of the color space and ds^2_{color} describes its geometry. Note that the line element suggested by Koenderink et al. is of this form:

$$ds^2 = dx^2 + dy^2 + \frac{1}{(R+G+B)^2}(dR^2 + dG^2 + dB^2). \tag{43}$$

We thus consider gradients at low intensity to be of greater importance than the same gradients at high luminosity.

The above line element is a special case of a local intensity normalization of a line element of the form

$$ds^2 = dx^2 + dy^2 + \beta(R+G+B)(dR^2 + dG^2 + dB^2). \tag{44}$$

The Levi-Civita coefficients are accordingly

$$\Gamma^i_{jk} = \beta^{-1}(\partial_k\beta\delta_{ij} + \partial_j\beta\delta_{ik} - \partial_i\beta\delta_{jk}). \tag{45}$$

In the case of the formalism proposed by Koenderink et al,

$$\beta^{-1}\partial_i\beta = -\frac{2}{A}, \tag{46}$$

where $A = R + G + B$. The Levi-Civita connection coefficients are

$$\Gamma^r_{ij} = -\frac{2}{A}\left(\delta_{ij} + \delta_{ik} - \delta_{jk}\right). \tag{47}$$

The second term of Koenderink's flow reads

$$\Gamma^r_{ij}\partial_\mu I^i \partial_\nu I^j g^{\mu\nu} = -\frac{2}{A}(2\partial_\mu I^r \partial_\nu A - \sum_{k=r,g,b} \partial_\mu I^k \partial_\nu I_k)g^{\mu\nu}. \tag{48}$$

We choose a less singular β as follows:

$$\beta(A) = C(\tanh(a(A-b)) + 1). \tag{49}$$

It is also more flexible and enables slightly better results. The Levi-Civita connection is

$$\beta^{-1}\partial_i\beta = \frac{2a}{3(e^{2A}+1)} \tag{50}$$

and, consequently, the second term of the red channel flow becomes

$$\begin{aligned}\Gamma^r_{ij}\partial_\mu I^i \partial_\nu I^j g^{\mu\nu} \quad = \quad & \frac{2a}{3(e^{2A}+1)}(g^{11}(R_x^2 - G_x^2 - B_x^2 + 2R_xG_x + 2R_xB_x) + \\ & 2g^{12}(R_xA_y + R_yG_x + R_yB_x - G_xG_y - B_xB_y) + \\ & g^{22}(R_y^2 - G_y^2 - B_y^2 + 2R_yG_y + 2R_yB_y))\end{aligned} \tag{51}$$

and, likewise, the other channels are obtained by proper cyclic permutations.

Another attractive possibility is to use the Buchsbaum coordinates, used also by Wolf et al. [17] for chromatic enhancement, and choose an intensity normalization function $\beta(k_1)$, such that for regions of high intensity β is large and the flow is less diffusive, while for low intensity regions β is small and the flow is diffusive. There are many reasonable choices for the function β. For the sake of illustration we use a combination of the logistic function:

$$\beta(k_1) = A(\tanh(a(k_1 - b)) + 1), \tag{52}$$

where the constants A, a and b are yet to be defined. The Levi-Civita coefficient is in this case

$$\Gamma^1_{11} = \beta^{-1}\partial_{k1}\beta = \frac{2a}{e^{2a(k_1-b)}+1}, \tag{53}$$

and all the other coefficients vanish. The second term of Eq. (12) is now equal to:

$$\Gamma^1_{ij}\partial_\mu X^i \partial_\nu X^j g^{\mu\nu} = \Gamma^1_{11}(g^{11}k_{1x}^2 + 2g^{12}k_{1x}k_{1y} + g^{22}k_{1y}^2). \tag{54}$$

Collecting all the terms we get the flow

$$\begin{aligned} k_{1t} &= \Delta_{g(\beta)}k_1 + \Gamma^1_{11}(g^{11}k_{1x}^2 + 2g^{12}k_{1x}k_{1y} + g^{22}k_{1y}^2) \\ k_{2t} &= \Delta_{g(\beta)}k_2 \\ k_{3t} &= \Delta_{g(\beta)}k_3. \end{aligned} \tag{55}$$

6 Experimental Results

6.1 Grey-Level

We present results obtained with our algorithm and compare them with those obtained by applying the Euclidean Beltrami flow. It is important to be reminded that there is an inherent difficulty associated with any attempt to compare the performance of two different flows. This is due to the lack of accepted objective criteria for assessing the effects of the image of a given algorithm. The evaluation is further complicated by the fact that it is task dependent. Yet it is rather easy to realize the differences between the flows by simply looking at the sequences $I(x, y, t)$ generated by two different algorithms.

We consider first Lenna's image preprocessed by an asymmetric "lateral illumination" effect obtained by adding a tilted plane to the image (Fig. 2).

The resultant Lenna image was processed with β in the form Eq. (35), with parameters chosen to be $b_1 = b_2 = 0$, $b_3 = 0.0025$ and $A = 3$. The derivatives of β with respect to the intensity can be done analytically while for the spatial derivatives of β and for those of the intensity we used the central differences scheme with a 3x3 kernel. We used an explicit Euler scheme for solving the partial differential equation. The result of the non-Euclidean flow after 20 iterations is compared with that obtained by using the Beltrami flow (Fig. 2).

As expected, and clearly depicted by the images of Fig. 2, our flow diffuses the brightest area of the image (particularly in the right side of the image) more rapidly than the Beltrami flow does. It is comparable in the center of the image, and diffuses slower in the darker regions, notably in the left side of the image.

6.2 Color

Our algorithm is demonstrated by using the sailboats image (Fig. 3). This is a color image constructed from a CCD camera by a de-mosaicing algorithm. We wish to filter out artifacts created in the process of de-mosaicing.

Using a low pass filter, e.g. the heat equation, for each channel separately, we obtain the sequence of images depicted in the upper row on Fig. 4. This filter does not preserve sharp edges and blur the image severely. We thus need an edge preserving

Figure 2: Processing of a grey-level image by the Beltrami flow. Upper-left: original 256x256 Lenna image. Upper-right: superposition of Lenna's image and a tilted plane. Lower-left: the recombined image (upper-left) after 20 iterations of the Beltrami flow. Lower-right: The recombined image after iterations of the non-Euclidean flow.

Figure 3: The original sailboats image constructed from a CCD camera by a de-mosaicing algorithm.

flow, i.e. the Beltrami flow (see Fig. 4 middle row). While in this case the results are much better than in the linear one, they still suffer from a drawback. Looking closely on the poles, one can see that instead of linear objects we get piecewise linear objects with very large and noticeable dislocations. These are artifacts of the compression that the Beltrami flow wrongly identifies as "true" edges and, therefore, does not smooth out.

We therefore need an algorithm that will smooth out the structure along the poles in a manner that a linear filter does, but will process everything else where according to the Beltrami flow. Our solution consists of using a non-Euclidean spatial-feature space whose metric is described by a Beta function that is very small over dark regions (i.e. $k_1 \approx 0$ or $R+G+B \approx 0$) and close to 1 elsewhere. Specifically, we choose

$$\beta(k_1) = A(\tanh(a(\tilde{k}_1 - b)) + 1), \tag{56}$$

with $A = 0.5$, $a = 0.05$ and $b = 10$. We extract β from a linearly smoothed image in order to have a smooth transition between regions with high and low values of β. The image was smoothed by 5 iterations of the linear heat equation with time step of $dt = 0.1$. The result obtained after one iteration of our highly non-linear flow with $dt = 0.05$ is presented in Fig. 7. A closer comparison of the poles between the Beltrami flow and our algorithm is depicted in Fig. 8.

The Beltrami flow is not scale invariant. The images shown in Fig. 6 illustrates the difference obtained in using $\beta = 1$ and $\beta = 5$ in the Stiles flow. Using the Scrödinger model of color perception results in a different flow. Snapshots of the flow which is based upon the Schrödinger model are depicted in Fig. 5.

7 Discussion

Many studies in vision and image sciences are oriented toward either global analysis (Bayesian, neural nets etc.) or local one (PDE, differential geometry etc.). Yet, it is

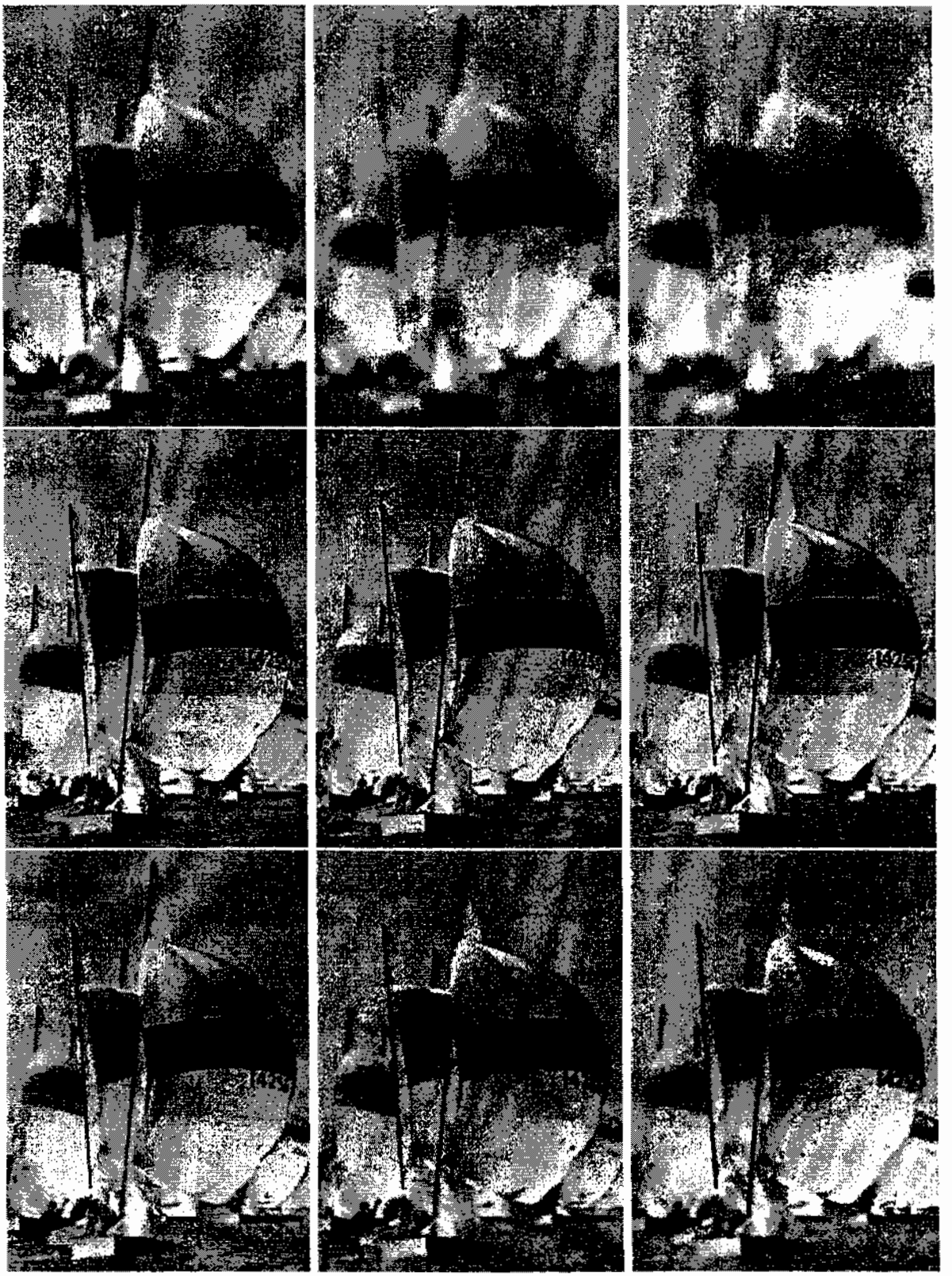

Figure 4: Results of applying a flow to the sailboats image after 4, 8, 12 iterations, from left to right, respectively. First raw: The Laplacian flow (heat equation). Second raw: The Euclidean RGB Beltrami flow. Third raw : The Stiles flow.

Figure 5: Image processing by the Schrödinger flow. Time (scale) is increasing from left to right.

clear that in most cases the performance of a global task (e.g. segmentation, identification) depends on the performance of the pre-processing and analysis stages. Likewise, the performance of local algorithms can be enhanced if an a priori knowledge about the class of images to be processed or the high-level task is given, and physical (e.g. illumination conditions) or psychophysical conditions are specified.

Rather than resorting to either the local or global approach, we propose in this study, to use the embedding space geometry within the framework of the Beltrami approach as a convenient and efficient interface between processing of global and local data. We presented in this paper only preliminary results that demonstrate the principles in the context of a simple setting. More realistic applications require further work in order to understand, by a combination of analytical and experimental methods, the right geometry of the embedding space which is appropriate for a given task. Other potentially powerful extensions may incorporates texture, depth and various invariance properties. These questions as well as the application of the proposed framework to medical images are under current investigation.

Acknowledgments

We wish to thank R. Kimmel for useful discussions, and help in the numerical implantation. This research has been supported in part by the Ollendorff Center, the Fund for Promotion of Research at the Technion, and by the Ministry of Science Vision Platform Project.

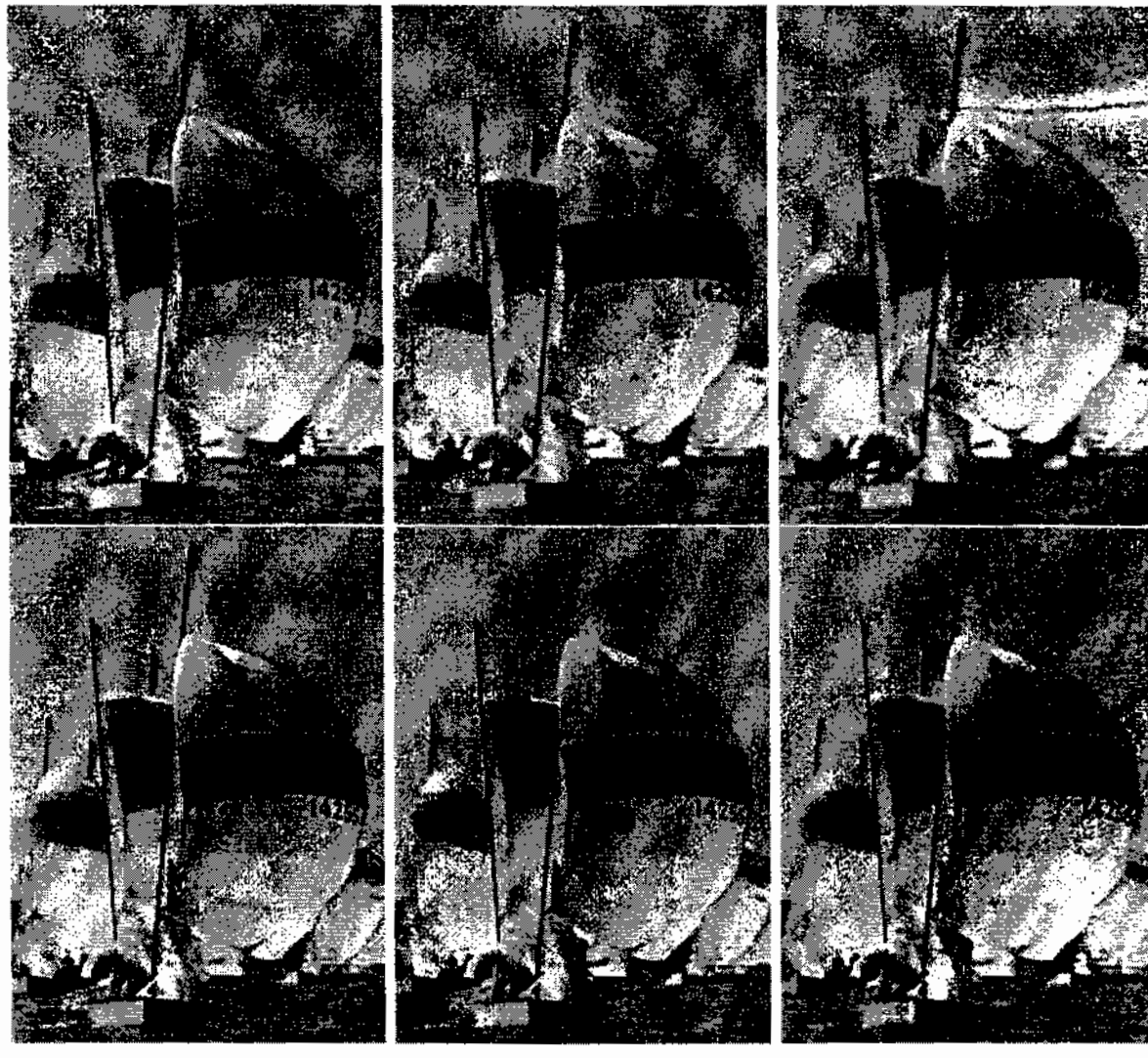

Figure 6: Results of applying a Stiles flow to the sailboat image after 4, 8, 12 iterations, from left to right, respectively. Upper row: Stiles flow with $\beta = 1$. Lower row: Stiles flow with $\beta = 5$

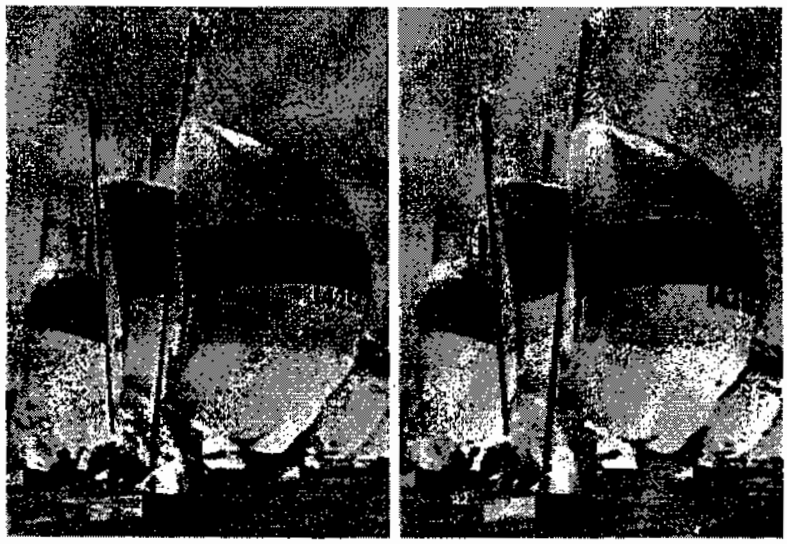

Figure 7: Left: The sailboats image after 200 iterations of the Euclidean Beltrami flow. Right: The same image obtained after one iteration of our adaptive smoothing algorithm, using a metric described by a logistic-type Beta function.

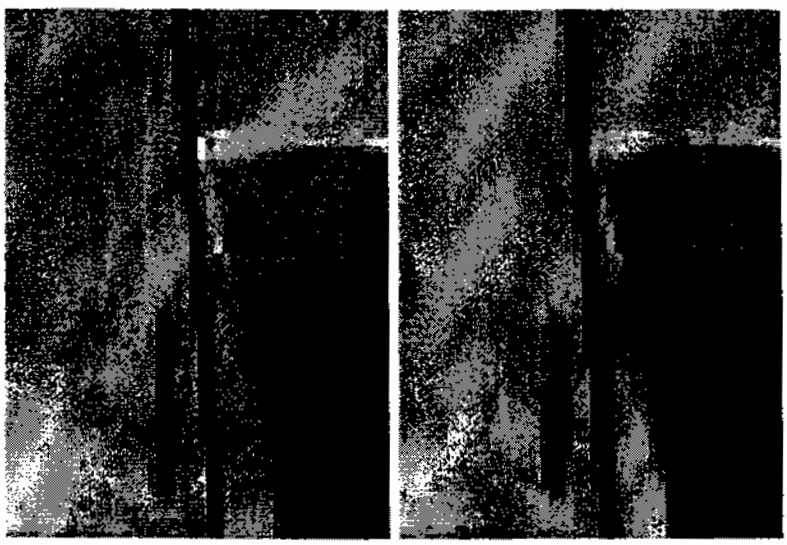

Figure 8: Comparison of the two smoothing algorithms illustrating their effects on the structure of the pole. Left: an enlarged part of the Beltrami smoothed image, Right: An enlarged part of the image obtained by application of our adaptive smoothing algorithm.

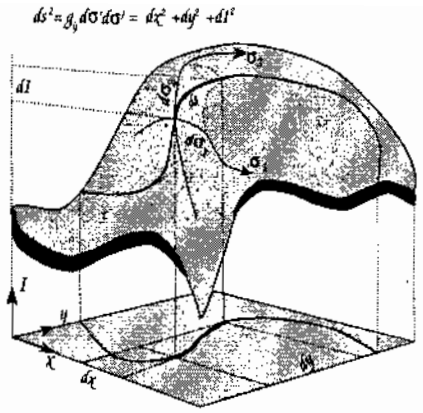

Figure 9: A length element of a surface curve ds may be either defined as a function of a local metric defined on the surface (σ_1, σ_2), or as a function of the coordinates of the space (x, y, I) in which the surface is embedded.

Appendix

A fundamental concept related to Riemannian differential geometry is distance. The natural question in this context is how do we measure distances? Consider first the important example of mapping $\mathbf{X} : \Sigma \to \mathbb{R}^3$. Denote the local coordinates of the two-dimensional manifold Σ by (σ^1, σ^2); these are analogous to arc length in the case of a one-dimensional manifold, i.e. a curve (Fig. 9). The map $\mathbf{X}$ specifies for each point (σ^1, σ^2) its 3D coordinates. The explicit form of $\mathbf{X}$ is given by $(X^1(\sigma^1, \sigma^2), X^2(\sigma^1, \sigma^2), X^3(\sigma^1, \sigma^2))$.

Since the local coordinates σ^i are curvilinear, the squared distance is given by a positive definite symmetric bilinear form, called the *metric*, whose components are denoted by $g_{\mu\nu}(\sigma^1, \sigma^2)$:

$$ds^2 = g_{\mu\nu} d\sigma^\mu d\sigma^\nu \equiv g_{11}(d\sigma^1)^2 + 2g_{12} d\sigma^1 d\sigma^2 + g_{22}(d\sigma^2)^2,$$

where we used Einstein summation convention in the second equality (i.e. identical indices that appear one up and one down are summed over). We denote the inverse of the metric by $g^{\mu\nu}$, so that $g^{\mu\nu} g_{\nu\gamma} = \delta^\mu_\gamma$, where δ^μ_γ is the Kronecker delta.

Let $\mathbf{X} : \Sigma \to M$ be an embedding of $(\Sigma, (g_{\mu\nu}))$ in $(M, (h_{ij}))$, where Σ and M are Riemannian manifolds and $(g_{\mu\nu})$ and (h_{ij}) are their respective metrics. We can use the knowledge of the metric on M and the map $\mathbf{X}$ to construct the metric on Σ. This procedure, formally denoted by $(g_{\mu\nu})_\Sigma = \mathbf{X}^*(h_{ij})_M$, is called for obvious reasons the *pullback*. It is given explicitly by:

$$g_{\mu\nu}(\sigma^1, \sigma^2) = h_{ij}(\mathbf{X}) \partial_\mu X^i \partial_\nu X^j, \tag{57}$$

where $i, j = 1, ..., \dim M$ are summed, and $\partial_\mu X^i \equiv \partial X^i(\sigma^1, \sigma^2)/\partial\sigma^\mu$.

Consider, for example, a grey level image which is, from our viewpoint, the embedding of a surface described as a graph in $\mathbb{R}^3$:

$$\mathbf{X} : (\sigma^1, \sigma^2) \to (x = \sigma^1, y = \sigma^2, z = I(\sigma^1, \sigma^2)), \tag{58}$$

where (x, y, z) are Cartesian coordinates. Using (10), we get

$$(g_{\mu\nu}) = \begin{pmatrix} 1 + I_x^2 & I_x I_y \\ I_x I_y & 1 + I_y^2 \end{pmatrix}. \tag{59}$$

This can be intuitively understood as follows: Eq. (10) means that the distance measured on the surface by the local coordinates is equal to the distance measured according to the embedding coordinate system (Fig. 9). Since the map $\mathbf{X}$ identifies x with σ^1 and y with σ^2, we can write

$$\begin{aligned} ds^2 &= dx^2 + dy^2 + dI^2 \\ &= dx^2 + dy^2 + (I_x dx + I_y dy)^2 \\ &= (1 + I_x^2)dx^2 + 2I_x I_y dx dy + (1 + I_y^2)dy^2. \end{aligned} \tag{60}$$

Note that one cannot tell by inspection of the metric by itself whether the surface or manifold in question is flat (Euclidean with no curvature) or not. In order to settle this issue, we need the concept of connection and Gaussian curvature.

Parallel transport and connections

In order the take derivatives of a vector field on a manifold we need to compare vectors at different points on the manifold. This becomes obvious from consideration of the heuristic formula

$$\frac{\partial V^i}{\partial x^j} = \lim_{\Delta x \to 0} \frac{V^i(..., x^j + \Delta x^j, ...) - V^i(..., x^j, ...)}{\Delta x^j}. \tag{61}$$

We see that the first term in the numerator is defined at $\mathbf{x} + \Delta\mathbf{x}$ while the second term is defined at $\mathbf{x}$. In order to have a meaningful expression we have to transport $\mathbf{V}(\mathbf{x})$ to $\mathbf{x} + \Delta\mathbf{x}$, *without a change*, and compute the difference. Since there is no natural way, in general, to do that, we have to specify how we perform this procedure, called **parallel transport**. Let $\tilde{\mathbf{V}}|_{x+\Delta x}$ denote a vector $\mathbf{V}|_x$ parallely transported to $\mathbf{x} + \Delta\mathbf{x}$. We demand that the components $\tilde{V}^i$ satisfy

$$\begin{aligned} \tilde{V}^i(x + \Delta x) - V^i(x) &\propto \Delta x, \\ (\widetilde{V^i + W^i})(x + \Delta x) &= \tilde{V}^i(x + \Delta x) + \tilde{W}^i(x + \Delta x). \end{aligned} \tag{62}$$

These conditions are satisfied if we take

$$\tilde{V}^i(x + \Delta x) = V^i(x) - V^k(x)\Gamma^i_{jk}\Delta x^j, \tag{63}$$

and the covariant derivative with respect to x^j is defined as

$$\lim_{\Delta x \to 0} \frac{V^i(..., x^j + \Delta x^j, ...) - \tilde{V}^i(..., x^j, ...)}{\Delta x^j} = \frac{\partial V^i}{\partial x^j} + \Gamma^i_{jk} V^k. \tag{64}$$

Different choices of Γ^i_{jk} correspond alternative means for executing the parallel transport.

Geodesics

Another way to understand the connection coefficients Γ^i_{jk} is as follows: Vector field components are given at any point, on the manifold of dimension N, in terms of N smooth and linearly independent vector fields. These N vector fields form, at each point, a linear basis-a frame for the tangent space at that point. The components of a given vector field are given with respect to this local frame. Frames at different points of the manifold are different in general. The connection describes how the frame is changed infinitesimally on the manifold. Denote by $e_i(\mathbf{x})$, $i = 1, ..., N$, the basis vectors of the space tangent to M at point $\mathbf{x}$. We can take, for example, the directions along the local coordinates $e_i = \partial/\partial x^i$. Denoting the covariant derivative by ∇, the change in the frame's vectors, when moved infinitesimally, in the direction of one of the vector basis, is

$$\nabla_i e_j = \nabla_{e_i} e_j = e_k \Gamma^k_{ij}. \tag{65}$$

Similarly, moving one vector in the direction of another vector is expressed by:

$$\begin{aligned} \nabla_V W &= V^i \nabla_{e_i}(W^j e_j) = V^i (e_i[W^j] e_j + W^j \nabla_{e_i} e_j) \\ &= V^i (\partial W^k / \partial x^j + W^j \Gamma^k_{ij}) e_k. \end{aligned}$$

Let now Σ be an interval $I = (a, b)$ and M some Riemannian manifold. The mapping $C : I \to M$ is a curve on M. Let W be a vector field along the curve and V the vector tangent to the curve:

$$V = \frac{d}{dt} = (\frac{dx^i(t)}{dt}) e_i. \tag{66}$$

If W satisfies

$$\nabla_V W = 0 \qquad \text{for any } t \in (a, b), \tag{67}$$

W is said to be parallely transported along $C(t)$. If the tangent vector itself is parallely transported along the curve C, that is, if

$$\nabla_V V = 0, \tag{68}$$

the curve $C(t)$ is called **geodesic**. In reference to the components, this equation reads

$$\frac{d^2 x^i}{dt^2} + \Gamma^i_{jk} \frac{dx^j}{dt} \frac{dx^k}{dt} = 0, \tag{69}$$

where x^i are the coordinates of $C(t)$.

The Levi-Civita Connection

The connection coefficients were up to this point arbitrary. We will now choose a special connection by adding a condition on the space of connections. Remember that the metric defines an inner product on the tangent space to a manifold. We demand that if two vectors X and Y are parallely transported along any curve on the manifold, then the inner product between them remains constant under parallel transport. Let

V be a tangent vector to some curve along which the vectors are parallely transported, then

$$\nabla_V(g_{ij}X^iY^j) = V^k\nabla_k(g)_{ij}X^iY^j = 0, \tag{70}$$

where we used the fact that X and Y are parallely transported (i.e. $\nabla_V X = \nabla_V Y = 0$). Since X, Y and V are arbitrary, we must have

$$\nabla_k(g)_{ij} = 0. \tag{71}$$

A connection that satisfies this condition is called *metric compatible*. At this point we will quote the result:

Theorem 1 (The fundamental theorem of Riemannian geometry) *Given a Riemannian manifold (M, g), there exists a unique symmetric connection which is compatible with the metric g. This connection is called the* **Levi-Civita Connection**. *Its components are given by the following expression*

$$\Gamma^i_{jk} = \frac{1}{2}g^{il}(\partial_j g_{lk} + \partial_k g_{jl} - \partial_l g_{jk}). \tag{72}$$

References

[1] G. Buchsbaum and A. Gottschalk. Trichrmacy, opponent colors coding and optimum color information transmission in the retina. *Proc. Roy. Soc. London Ser. B*, 220:89–113, 1983.

[2] H. Helmholtz von. *Handbuch der Psychologishen Optik*. Voss, Hamburg, 1896.

[3] J. Kacur and K. Mikula. Slow and fast diffusion effects in image processing- Approximation schemes and numerical experiments. preprint No. 96-26 IWR, Heidelberg University, Germany, April, 1996.

[4] R. Kimmel R. Malladi and N. Sochen. Images as embedded maps and minimal surfaces: Movies, color, texture, and volumetric medical images. LBNL ,UC and TAUHEP Report LBNL-40490, UC-405, June 1997.

[5] J. Koenderink et al. *Kibernetik*, 6:227–237, 1970.

[6] D. L. MacAdam. Visual sensitivity to color differences in daylight. *J. Opt. Soc. Am.*, 32:247, 1942.

[7] D. L. MacAdam. Specification of small chromaticity differences. *J. Opt. Soc. Am.*, 33:18, 1943.

[8] A. M. Polyakov. Quantum geometry of bosonic strings. *Physics Letters B*, 103B(3):207–210, 1981.

[9] G. Sapiro and D. L. Ringach. Anisotropic diffusion of multivalued images with applications to color filtering. *IEEE Trans. Image Proc.*, 5:1582–1586, 1996.

[10] E. Schrödinger. Grundlinien einer theorie der farbenmetrik in tagessehen. *Ann. Physik*, 63:481, 1920.

[11] N. Sochen, R. Kimmel, and R. Malladi. From high energy physics to low level vision. Report LBNL 39243, LBNL, UC Berkeley, CA 94720, August 1996.

[12] N. Sochen R. Kimmel and R. Malladi. A general framework for low level vision. *IEEE Trans. IP*, 7:310, 1998.

[13] N. Sochen and Y.Y. Zeevi. *in preparation*, 1998.

[14] N. Sochen and Y.Y. Zeevi. Representation of Colored Images by Manifolds Embedded in Higher Dimensional Non-Euclidean Space *ICIP98*, 1998.

[15] W. S. Stiles. A modified Helmholtz line element in brightness-color space. *Proc. Phys. Soc. (London)*, 58:41, 1946.

[16] J. J. Vos and P. L. Walraven. An analytical description of the line element in the zone-fluctuation model of color vision II. The derivative of the line element. *Vision Research*, 12:1345–1365, 1972.

[17] S. Wolf R. Ginosar and Y. Y. Zeevi. Spatio-Chromatic image enhancement based on a model of human visual information processing. *J. Vis. Com. Im. Rep.* . 9:25–37, 1998.

[18] G. Wyszecki and W. S Stiles. *Color Science: Concepts and Methods, Qualitative Data and Formulae, (2nd edition).* John Wiley & Sons, 1982.

[19] Y. Y. Zeevi, R. Ginosar and O. Hilsenrath. Wide dynamic range camera. *U.S.A. patent No. 5,144,442*, 1992.

[20] Y. Y. Zeevi, R. Ginosar and O. Hilsenrath. Dynamic image representation system. *U.S.A. patent No. 5,420,637*, 1995.

The *Center for Communication* is managed by the

Department of Electrical Engineering.

This Technical Report is listed also as

EE PUB #1181, November, 1998.